Structural Plasticity in the Topology of the Membrane-Interacting Domain of HIV-1 gp41

Alexander Kyrychenko,[†] J. Alfredo Freites,[‡] Jing He,[§] Douglas J. Tobias,[‡] William C. Wimley,[§] and Alexey S. Ladokhin[†*]

[†]Department of Biochemistry and Molecular Biology, The University of Kansas Medical Center, Kansas City, Kansas; [‡]Department of Chemistry, University of California, Irvine, California; and [§]Department of Biochemistry, Tulane University School of Medicine, New Orleans, Louisiana

ABSTRACT We use a number of computational and experimental approaches to investigate the membrane topology of the membrane-interacting C-terminal domain of the HIV-1 gp41 fusion protein. Several putative transmembrane regions are identified using hydrophobicity analysis based on the Wimley-White scales, including the membrane-proximal external region (MPER). The MPER region is an important target for neutralizing anti-HIV monoclonal antibodies and is believed to have an interfacial topology in the membrane. To assess the possibility of a transmembrane topology of MPER, we examined the membrane interactions of a peptide corresponding to a 22-residue stretch of the MPER sequence (residues 662–683) using fluorescence spectroscopy and oriented circular dichroism. In addition to the previously reported interfacial location, we identify a stable transmembrane conformation of the peptide in synthetic lipid bilayers. All-atom molecular dynamics simulations of the MPER-derived peptide in a lipid bilayer demonstrate a stable helical structure with an average tilt of 24 degrees, with the five tryptophan residues sampling different environments inside the hydrocarbon core of the lipid bilayer, consistent with the observed spectral properties of intrinsic fluorescence. The degree of lipid bilayer penetration obtained by computer simulation was verified using depth-dependent fluorescence quenching of a selectively attached fluorescence probe. Overall, our data indicate that the MPER sequence can have at least two stable conformations in the lipid bilayer, interfacial and transmembrane, and suggest a possibility that external perturbations can switch the topology during physiological functioning.

INTRODUCTION

The gp160 envelope glycoprotein of HIV is composed of two proteins, gp120, which is responsible for binding to cell surface receptors, and gp41, which drives fusion of the viral and cellular membranes. gp41 is an integral membrane protein with a large highly conserved membrane interacting C-terminal domain, the exact topology of which remains controversial (1,2). A recent review from Steckbeck and co-authors identified two alternative models for the membrane-spanning sequences of HIV gp41 (1): a) the traditional model, with the membrane-spanning domain (MSD) as single transmembrane (TM) α-helix comprising residues 684–705 (illustrated in Fig. S1, *left panel*, in the Supporting Material) and b) the alternative model proposed by Hollier and Dimmock (3) in which the MSD spans the membrane in three β-strands (Fig. S1, *right panel*). Although the former model does not appear to explain all of the experimental evidence (e.g., the topology of the Kennedy epitope (KE) (4)), the latter, as discussed below, appears to violate the basic thermodynamic principles of protein-membrane interactions. The sequence hydrophobicity analysis presented here identifies additional putative membrane-spanning helical segments, which can potentially reconcile the accessibility data in the literature. One such segment is adjacent to the TM sequence in the traditional model and until now has been considered to have an interfacial topology in the context of the entire protein. This aromatic-rich sequence covering residues 662–683 is referred to as the membrane proximal ectodomain region (MPER), which is an important target for neutralizing anti-HIV monoclonal antibodies (5,6). From here on in this work, we use an extended definition of MSD, which in addition to previously suggested TM segments (Fig. S1) includes MPER and other hydrophobic regions and covers the segment of sequence from residue 660 to residue 820.

A series of biophysical studies carried out with the isolated peptide with the sequence derived from the MPER region (MPER peptide: Acetyl-ELDKWASLWNWFDITNWLW YIK-Amide) identified an interfacial (IF) location of this peptide, when it is added externally to preformed lipid vesicles (5). The neutralizing activity of anti-MPER antibodies may depend on its state of association with membranes (7,8). Here, we identify a new, to our knowledge, TM conformation of the MPER peptide, which is populated when vesicles are formed in the presence of the peptide. We use various spectroscopic tools, molecular dynamics (MD) simulations, and hydrophobicity analysis based on Wimley-White scales (9) to characterize the structure and thermodynamics of membrane interactions of MPER peptide. We suggest that in the context of the entire gp41 protein the conformational plasticity of MPER sequence could have important

Submitted July 24, 2013, and accepted for publication December 23, 2013.

*Correspondence: aladokhin@kumc.edu

Alexander Kyrychenko's present address is V.N. Karazin Kharkiv National University, Kharkiv, 61022, Ukraine.

Editor: Paulo Almeida.

0006-3495/14/02/0610/11 $2.00

http://dx.doi.org/10.1016/j.bpj.2013.12.032

physiological implications for membrane destabilization in the course of viral fusion, and to our knowledge, could be important for the design and engineering of novel antibody-based therapeutics.

EXPERIMENTAL SECTION

Materials

1-Palmitoyl-2-oleoyl-*sn*-glycero-3-phosphocholine (POPC), 1-palmitoyl-2-oleoyl-*sn*-glycero-3-phospho-glycerol (POPG), cholesterol, 1-palmitoyl-2-stearoyl-(*n*–Doxyl)-*sn*-glycero-3-phosphocholine (*n*–Doxyl–PC), and 1-palmitoyl-2-oleoyl-*sn*-glycero-3-phospho-(TEMPO)choline (Tempo-PC) spin-labeled lipids were obtained from Avanti Polar Lipids (Alabaster, AL). The MPER peptide, corresponding to the gp41 sequence segment 662–683, and its single cysteine mutant W666C (we retain the numeration of the parent sequence for the entire protein) were produced as described in (5). To prepare MPER/large unilamellar vesicles (LUV) samples, either unlabeled MPER peptide or NBD-labeled mutant (MPER-W666C-NBD) were codissolved in a methanol/chloroform mixture with corresponding lipids and then dried under a high vacuum for ~12 h. The dried lipid mixtures were dissolved in 50 mM sodium phosphate buffer pH 8 and vortexed to disperse the lipids. LUVs of 0.1 μm diameter were prepared by extrusion (10). Lipid concentrations of stock solutions were determined according to the procedure of Bartlett (11).

Fluorescence measurements

Fluorescence was measured using a SPEX Fluorolog FL3-22 steady-state fluorescence spectrometer (JobinYvon, Edison, NJ) equipped with double-grating excitation and emission monochromators. The measurements were made in a cuvette with a 2-by-10 mm optical path oriented perpendicular to the excitation beam and maintained at 25°C using a Peltier device from Quantum Northwest (Spokane, WA). For the Trp fluorescence measurements an excitation wavelength 280 nm was used and the slits were 3 nm on excitation and 5 nm on the emission path. For the NBD measurements the excitation wavelength was 465 nm and the slits were 5 nm. All spectra were corrected for spectral sensitivity of the detector as described (12) and the background signal was subtracted.

Fluorescence decays were measured with a time-resolved fluorescence spectrometer, FluoTime 200 (PicoQuant, Berlin, Germany), using a standard time-correlated single-photon counting scheme. For the lifetime measurements the samples were excited at 375 nm by a subnanosecond pulsed diode laser, LDH 375 (PicoQuant), with a repetition rate of 10 MHz. Fluorescence emission was detected at 535 nm, selected by a Sciencetech model 9030 monochromator, using a PMA-182 photomultiplier (PicoQuant). The fluorescence intensity decay was analyzed using FluoFit iterative-fitting software based on the Marquardt algorithm (PicoQuant). The data were fit to a double exponential decay as described (13) and amplitude-averaged times were calculated to characterize quenching-associated reduction in excitation lifetime.

For fluorescence measurements of MPER+LUV, the peptide concentration was 1–2 μM. For MPER/LUV, the peptide concentration was 2 μM, and the POPC concentration was 0.5–2 mM. For depth-dependent quenching experiments, 30 mol % of spin-labeled lipids in 0.5 mM POPC matrix were used, and the concentration of NBD-labeled MPER was 0.5 μM.

Circular dichroism (CD) measurements

Solution CD measurements were performed using an upgraded Jasco-720 spectropolarimeter (Japan Spectroscopic, Tokyo). Normally, 50–80 scans were recorded between 190 and 260 nm with a 1 nm step at 25°C using a 1 mm optical path cuvette. The sample contained 5 μM of MPER peptide and 1 mM POPC LUV, when present. To prepare oriented CD samples, lipid and peptide (MPER, melittin, or MelP5 melittin analog) were codissolved in methanol at 20 mg/ml lipid and a 1:200 peptide/lipid molar ratio. Onto a 1 cm^2 quartz disc, we applied a total of 25 μl of the lipid peptide mixture, allowing for the solvent to dry almost fully between each 5 μl addition. After addition of all 25 μl, the solvent was completely dried from the film and the disc was assembled into an airtight cylindrical sample holder with a second quartz window. A 100 μl drop of water was placed inside the sample holder, but not in contact with the sample, to hydrate the lipid-peptide film through the vapor phase and generate stacked oriented multibilayers. After at least 2 h of hydration the sample was placed in the beam of a Jasco 810 Circular Dichroism Spectropolarimeter with the lipid peptide film perpendicular to the beam. CD spectra were collected at six 60° rotations of the sample around the beam axis and the average was taken. The lipid-only spectra for both solution and oriented CD were collected in exactly the same way and then subtracted.

Analysis

Energetics of membrane partitioning

Relative changes in fluorescence intensity at constant wavelength, I, were measured as a function of lipid concentration and fit to the following equation (12):

$$I = 1 + I_{max} K_p [L] / \left([W] + K_p [L] \right), \quad (1)$$

where I_{max} = the maximal fluorescence increase on the complete partition, [L] = the molar concentration of lipid,

[W] = the molar concentration of water (55.3 M), K_p = the mole fraction partition coefficient. The Gibbs free energy ΔG of transfer from water to a lipid membrane was calculated from the mole fraction partition coefficients K_p:

$$\Delta G = -RT \ln K_p. \quad (2)$$

Distribution analysis (DA) of depth-dependent fluorescence quenching

In membrane quenching experiments, a series of samples with *n*-Doxyl-PC spin quenchers at various depths were used to quench the fluorescence of an NBD dye attached at a unique cysteine residue of the W666C MPER mutant (MPER-W666C-NBD). Fluorescence lifetime changes were used to generate a depth-dependent fluorescence quenching profile $\tau_0/\tau(h)$-1, where τ_0 is the average lifetime in the absence of quencher and $\tau(h)$ is the lifetime in the presence of the quencher located at depth h, defined as the transverse distance from the bilayer center (14). The quenching data were analyzed by using the DA methodology (15–17), which approximates the transverse quenching profile with a Gaussian function of depth $G(h)$:

$$G(h) = \frac{S}{\sigma\sqrt{2\pi}} \exp\left[-\frac{(h-h_m)^2}{2\sigma^2}\right], \quad (3)$$

where h_m = the center (mean) of the quenching profile, σ = the width of the distribution, and S = the area of the quenching profile. To account for *trans*-leaflet quenching of the deeply penetrating NBD fluorophore, a symmetrical second Gaussian, $G(-h)$, is added to the fitting function (16). Note that either single or coupled double Gaussian fits use only three fitting parameters: h_m, σ, and S, corresponding to the most probable depth of penetration, fluctuations in the transverse position, and overall accessibility to quenching (i.e., quenching efficiency), respectively.

MD simulation setup

To setup the simulation system, one MPER peptide in an ideal α-helical conformation was inserted across a POPC bilayer in excess water prepared with the CHARMM-GUI membrane builder (18). The lipid molecules from each bilayer leaflet that overlapped with the peptide were removed from the system. The final system consisted of the peptide, 72 POPC lipid molecules (36 in each bilayer leaflet), and 2,730 waters for a total of 18,252 atoms.

The initial configuration was subjected to 100 steps of conjugate-gradient energy minimization followed by 200 ps at constant volume and constant temperature (303 K) during which all the peptide atoms were held fixed. Following these initial preequilibration steps, the positional restraints on the MPER atoms were removed, and the production run was carried out for 110 ns at constant pressure (1 atm) and temperature (303 K). A second 504-ns simulation trajectory was generated at 393 K and 1 atm starting from the end configuration of the 303 K trajectory.

The simulations were run with the NAMD software package (19). The peptide was modeled using the CHARMM22 and CHARMM36 protein force fields (20–22) in the 303 K and 393 K simulations, respectively. The CHARMM36 force field was used for lipids (23) and the TIP3P model (24) was used for waters. A reversible multiple-time-step algorithm (25) was used to integrate the equations of motion with a time step of 4 fs for the long-range electrostatic forces, and 2 fs for the short-range nonbonded forces and the bonded forces. The smooth particle mesh Ewald method (26) was used to calculate electrostatic interactions. The short-range interactions were cutoff at 12 Å using a force-based switching scheme. All bond lengths involving hydrogen atoms were held fixed using the SHAKE (27) and SETTLE (28) algorithms. A Langevin dynamics scheme was used for thermostating. Nosé-Hoover-Langevin pistons were used for pressure control (29,30). Simulation analyses were generated using the Gromacs (31) and VMD (32) software packages.

RESULTS AND DISCUSSION

See Fig. 1 *A* for an illustration of the main observation that identified conformational plasticity of the MPER peptide in lipid bilayers, which compares the tryptophan spectrum of the peptide in solution (*black*) to that in two different preparations of peptide associated with the LUV made of POPC. The first preparation, designated as MPER+LUV (*blue*), represents conditions when peptide is added to preformed vesicles, whereas the second one, designated MPER/LUV (*red*), is obtained by co-extruding vesicles in the presence of peptide, which had been mixed with the lipid in organic solvents before hydration and formation of vesicles. Clearly the two samples have dramatically different spectroscopic signatures, with the spectrum of the MPER/LUV sample being substantially blueshifted, indicating a much more hydrophobic average environment of the peptide's five tryptophan residues. The samples retained their spectral properties even after several days of incubation at room temperature. This result cannot be explained merely by insufficient membrane association of the peptide in MPER+LUV sample, as the fluorescence intensity titration experiment (Fig. S2) indicates a strongly favorable association of MPER with POPC LUV, with a free energy of partitioning, ΔG, in excess of −8 kcal/mol. For reference, the partitioning of MPER peptide into the zwitterionic POPC bilayer is stronger than that of the well-studied membrane-active peptide melittin (33,34). Thus, the spectrum of the MPER+LUV sample in Fig. 1 *A* corresponds to the fraction of membrane-associated peptide being over 95%.

To further investigate spectral heterogeneity of the MPER peptide, we have fit the spectra with a log-normal

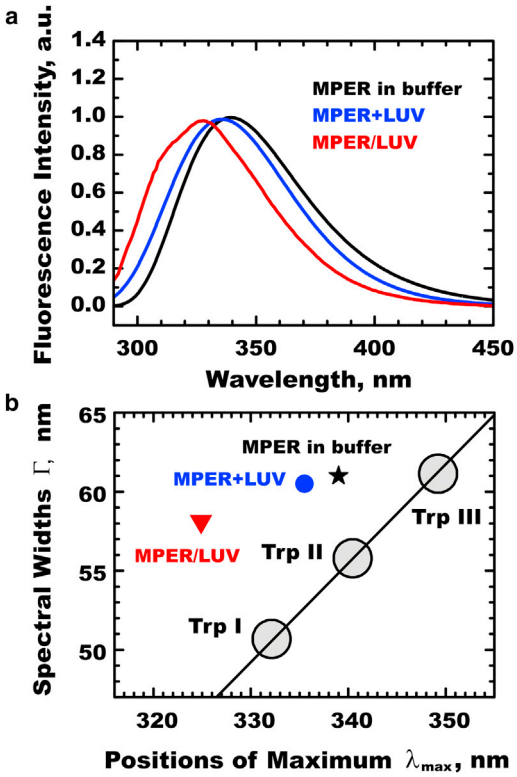

FIGURE 1 Analysis of tryptophan fluorescence of the MPER peptide in various membranous complexes. (*a*) Normalized corrected spectra of the MPER peptide in solution (*black*), added to preformed POPC vesicles (MPER+LUV, *blue*) and coextruded with POPC vesicles (MPER/LUV, *red*). Peptide and lipid concentration were 2 μM and 1 mM, respectively. (Identical spectra were measured with lipid concentrations of 0.5 and 2 mM.) (*b*) Position-width analysis of Trp fluorescence of MPER samples (*symbols*). Large circles labeled Trp I, Trp II, and Trp III show the classes of tryptophan residues that correlated roughly with the extent of water exposure (see text for details). To see this figure in color, go online.

distribution (12,35,36) and plotted the recovered spectral width as a function of the spectral maximum (Fig. 1 *B*). For the MPER in solution and MPER+LUV samples we observe noticeable spectral broadening, which is identified as an upward deviation from the linear baseline that can be drawn through position-width points corresponding to spectral classes I, II, and III identified by Burstein and coworkers (35,36). (The difference between these three classes can be attributed to the variations in dipolar relaxation of the solvation shell during the excited state lifetime: III-fast relaxation, II-slow relaxation, I-no relaxation.) The spectra of MPER in buffer (*black symbol*) and MPER+LUV (*blue symbol*) fall on a characteristic semi-arc (not shown) connecting classes I and III, indicating that the spectra of these samples comprise the mixtures of the named two spectral classes, with a possible contribution from class II. Note that the spectrum of a single Trp residue of the peptide melittin interfacially bound to POPC LUV belongs to class I (12). In contrast, the position-width point for MPER/LUV (Fig. 1 *B*, *red symbol*) is more blueshifted as compared to class I, indicating the contribution of the relatively seldom-observed tryptophan spectral classes A and S. In soluble proteins these classes are associated with an extremely apolar environment of the indole ring, not only eliminating dipolar relaxation (as in class I), but preventing formation of the hydrogen bond complex in the excited state of indole fluorophore of tryptophan (37–40). The relatively large spectral width of MPER/LUV (as compared to a linear baseline through classes I, II, and III) is indicative of substantial heterogeneity in the environments of the five Trp residues of MPER, which is consistent with a TM rather than an IF orientation.

CD measurements reveal further differences in conformation of the peptide in the two types of preparation of membrane-associated MPER (Fig. 2). The CD spectrum of the MPER/LUV sample (*red*) obtained by coextrusion with POPC has two negative peaks, generally consistent with a helical conformation. The variation from a canonical helical spectrum is likely to be related to the presence of multiple tryptophans, which can produce strong exciton splitting when placed in the restrictive hydrophobic environment of lipid bilayer (e.g., similar to that observed for another tryptophan-rich peptide, indolicidin (41)). In contrast, when MPER peptide is added to preformed vesicles (MPER+LUV sample, *blue line* in Fig. 2), the CD spectrum is dominated by a single negative peak at ~215 nm characteristic of beta structure. The same spectrum is also observed for the MPER peptide injected into buffer from organic solvent (not shown) and is likely related to the formation of peptide aggregates, which is not surprising for such a hydrophobic sequence. It is worth mentioning that the previously suggested partially helical conformation of the IF MPER peptide is based on NMR measurements performed in the presence of detergent micelles rather than lipid bilayers (5,6). Similarly, CD spectra collected in membrane mimetics, such as detergents and organic solvents, are consistent with partially helical structure (Fig. S3).

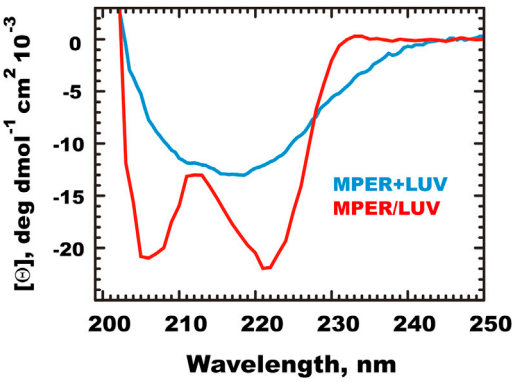

FIGURE 2 CD of the MPER peptide in various membranous complexes: added to preformed POPC vesicles (MPER+LUV, *blue*) and coextruded with POPC vesicles (MPER/LUV, *red*). Peptide and lipid concentration were 5 μM and 1 mM, respectively. To see this figure in color, go online.

We have also examined the orientation of the MPER peptide in hydrated oriented multilayers of POPC by means of oriented circular dichroism (OCD) (42). The samples for OCD are made by cosolubilization of lipid and peptide in organic solvent with subsequent deposition on a flat quartz slide, and hydration through the vapor phase. This is very similar to the preparation of the MPER/LUV sample, lacking the extrusion of vesicles. We compare the OCD spectra of MPER to that of melittin and a recently discovered melittin mutant, MelP5 (43), with a TM topology, after identical preparation of the samples (Fig. 3). As expected (43,44), native melittin gives a typical OCD spectrum for an IF helix, with two large minima. MPER gives a much weaker single minimum, very similar to that of the TM peptide MelP5 and other TM α-helices (42,43).

To examine the conformation and orientation of the TM form of MPER in the membrane, we performed a MD simulation of a single MPER peptide in a fully hydrated POPC bilayer (Fig. 4). Because of the enormous thermodynamic penalty for partitioning of an unfolded polypeptide chain into the hydrocarbon core of the lipid bilayer (45–47), the peptide was modeled initially as an ideal α-helix. After a 110 ns unrestrained trajectory, the MPER retains helical conformation (Fig. 4) and a relatively narrow distribution of peptide tilt angle, centered at 24° with respect to the bilayer normal (Fig. S4), which allows for the optimal hydrophobic matching of the peptide and hydrocarbon core. To ensure that our system is not stuck in a kinetically trapped state, we performed a second MD simulation at elevated temperature to 393 K for an additional 504 ns (Fig. 4). This simulation revealed only a marginal decrease in secondary structure and a slightly broadened tilt distribution centered at 23° (Fig. S4). Our MD simulations also revealed formation of a persistent salt bridge between K665 and acidic residues E662 and D664 (Fig. S5).

We have plotted the transverse distributions of each of the five Trp residues and compared them with the distributions

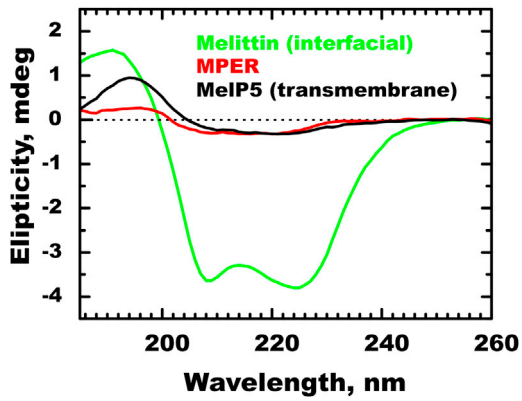

FIGURE 3 OCD spectra of the MPER peptide in hydrated POPC multilayers (*red*) compared to those of the interfacially oriented melittin (*green*) and its MelP5 mutant with a TM orientation (*black*) (43). In all cases lipid/peptide ratio was 200. To see this figure in color, go online.

of acyl chains, lipid phosphate groups, and interfacially penetrating water molecules in Fig. 5 *A*. Although the environment of the central residue W672 is completely hydrophobic, the flanking residues, W666 and W680, can interact with polar groups and water. Such structural heterogeneity can easily explain the spectral behavior of the Trp fluorescence in the MPER/LUV sample (Fig. 1). Note that both flanking Trp residues are inserted deeper than the level of the lipid phosphates, which are normally taken as a hallmark of the interface, e.g., in depth-dependent electron paramagnetic resonance measurements. Indeed, the depth of the bilayer penetration for spin probes attached to cysteine residues placed at different positions in MPER peptide was found to be much shallower (48) in samples prepared by adding peptide to preformed vesicles (5).

To verify the features of the MPER penetration revealed by the MD simulation, we prepared a single cysteine mutant of the peptide, replacing W666, and labeling it with an NBD fluorophore. This peptide enables us to conduct a selective depth-dependent fluorescence quenching experiment of this fluorophore using lipid-attached doxyl probes (49). We chose this particular replacement for two reasons: a) substituting Trp with NBD-labeled Cys roughly preserves the size and results in replacement of one heterocyclic moiety with another, and b) based on our MD estimates this should position the fluorophore at a particular depth in the bilayer, where it can be reliably probed by multiple lipid-attached quenchers (14). First, we verified that this replacement of Trp with Cys-attached NBD does not grossly perturb the overall nature of the interaction with the POPC bilayer, by reproducing the lipid titration experiment, which gave excellent correspondence (compare free energies of partitioning in Fig. S2, *panels a and c*).

Depth-dependent fluorescence quenching allows one to estimate the membrane penetration of a fluorophore attached to a site of interest on a protein or peptide by measurements of the changes in intensity or lifetime upon addition of the lipid-attached quenchers of known depth. Here, we have used fluorescence lifetime measurements for a series of MPER/LUV samples where we incorporated into POPC matrix identical fractions of the lipids labeled with doxyl probes attached along the *sn*-2 acyl fatty chain at positions 5, 7, 10, 12, or 14, respectively. Lifetime measurements are more reliable than standard intensity measurements, as they are independent of the concentration of the fluorophores, and hence are better suited for membrane studies dealing with hydrophobic sequences subject to losses due to precipitation (50,51). We have used the DA methodology (Eq. 3) (15,16,52), which has recently been validated using MD simulations (17), for quantitative analysis of quenching. In this procedure experimental quenching profiles are fit to a symmetrical sum of two mirror-image Gaussian distributions, each representing penetration into a single leaflet, see illustration in Fig. 5 *B*. The lifetime quenching data are shown as symbols, and the principle

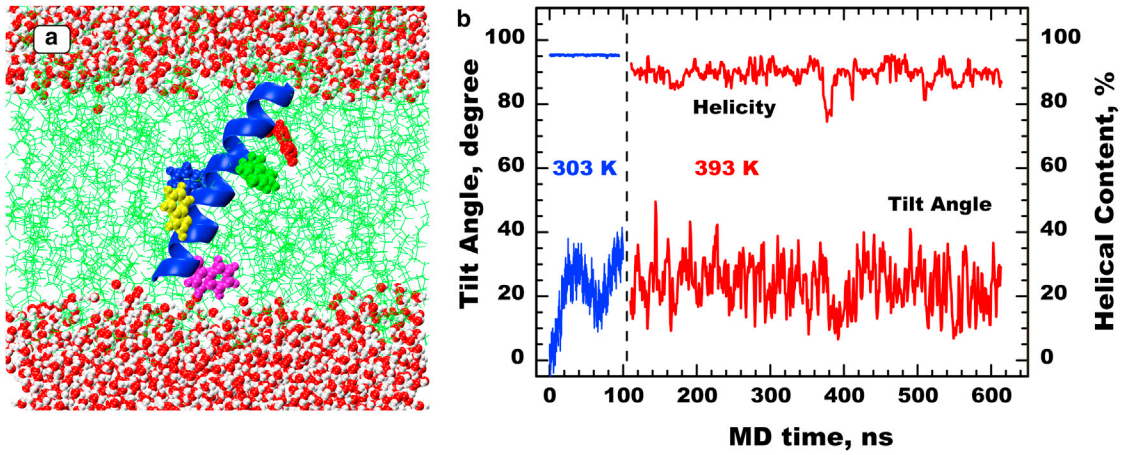

FIGURE 4 (*a*) Configuration snapshot from an all-atom MD simulation of the MPER peptide inserted into a POPC bilayer. The POPC bilayer is depicted in green and water molecules are shown as red balls. The peptide backbone is shown as a blue ribbon and the five Trp residues are shown in space-filling representation and are color-coded as noted in Fig. 5. (*b*) Helical content and tilt of the MPER peptide over two MD simulations carried out at 303 K (*blue traces*) and 393 K (*red traces*). To see this figure in color, go online.

Gaussian distribution for the quenching profile of NBD attached to W666C mutant of MPER peptide is highlighted, with the mirror-image shown as dotted line. The recovered distribution has an average transverse position of ~6 Å from the center of the bilayer and a substantial width due to the thermal motion. It is very close to the average distribution of the W666 from MD simulation (compare highlighted distributions in Fig. 5, *A* and *B*), providing reasonable experimental validation of our MD simulation. The resulting penetration is very different from the IF penetration of NBD attached to the lipid headgroup estimated by the same methodology (51). The estimated average depth of 6 Å for W666C-NBDin MPER/LUV also differs substantially from that of the same residue labeled by a spin probe in an electron paramagnetic resonance experiment conducted with the peptide added to preformed vesicles (an equivalent of MPER+LUV sample), which positions it close to the phosphate groups at ~20 Å from bilayer center (5). Taken together these data confirm our result highlighted in Figs. 2–4, which shows the conformational plasticity of the MPER peptide: it forms an IF structure when added to preformed vesicles (MPER+LUV sample) and a TM helix when membranes are formed in the presence of the peptide (MPER/LUV sample).

Next, we used tryptophan fluorescence to examine whether variations in lipid compositions would have an effect on the membrane interactions of the MPER peptide. We detected no variation in the spectral shape of emission for the samples in which the peptide was added to preformed LUV (not shown). In contrast, the spectral properties of the coextruded samples were affected by the presence of cholesterol and POPG lipid (Fig. 6). In both cases the spectral positions fall between those observed for the MPER/POPC (putative TM conformation) and the MPER+LUV samples (putative IF conformation). Assuming that lipid variation affects the relative proportion of the two conformations rather than their spectral signatures, we have decomposed the spectra measured in the presence of cholesterol and POPG into two components (Fig. 6, *shaded areas*). Our results suggest that stiffening the bilayer with cholesterol somewhat reduces the fraction of the peptide in a TM conformation, whereas introduction of negatively charged POPG makes both conformations approximately equally probable.

We analyze the thermodynamic reasons behind the conformational plasticity of the MPER sequence on the membranes using a general methodology outlined in the work of White and co-workers (46,47,54). Fig. 7 summarizes the application of the MPEx web tool (http://blanco.biomol.uci.edu/mpex/ (55)) based on the Wimley-White hydrophobicity scales (9) to the prediction of membrane-interacting segments in proteins. The advantage of these scales is that they are experimental absolute value free energy scales, i.e., they have zero free energy reference points. This implies that any single point in a hydropathy trace obtained with a 19-residue sliding window that is above zero level corresponds to a favorable TM conformation of a 19-residue helix, centered at this residue (Fig. 7 *A*). The quantitative application of the octanol scale for prediction of potential TM helical segments has been verified by statistical analysis of known TM segments (56) and normally requires only a marginally small adjustment for the estimate of backbone partitioning (the small value of this adjustment has been recently verified experimentally (57)). Another advantage of this scale is that it allows separate estimates to be made for the protonation states of residues such as D and E (*compare yellow and red traces*). As indicated by the results in Fig. 7 *A*, the MPER sequence resides within a large hydrophobic segment (*highlighted as a horizontal bar for each protonation state of acidic residues*), long enough to potentially include

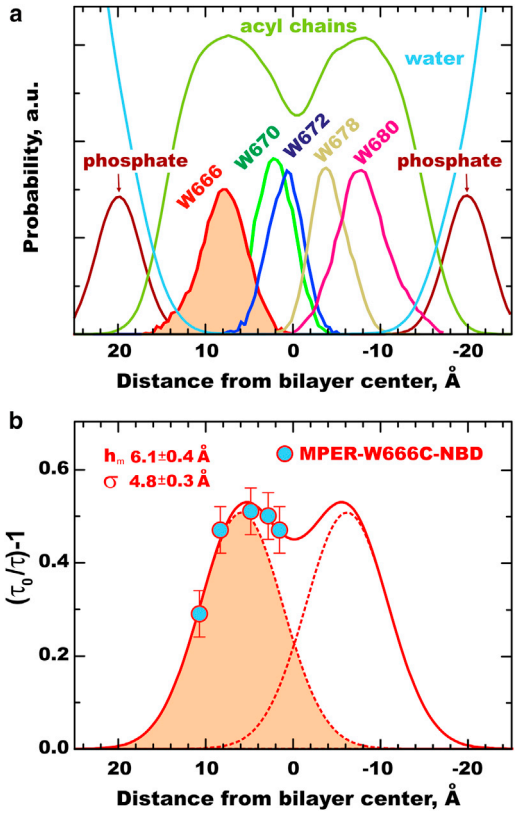

FIGURE 5 Identification of the transmembrane configuration of MPER by MD simulations and fluorescence quenching. (*a*) Mass density distribution of the MPER peptide Trp residues along the TM direction (303 K MD run). The Trp distributions are superimposed with the distribution of the lipid acyl chains (*green*), forming the hydrophobic core of the lipid bilayer. The distributions of the lipid phosphate groups (*wine*) and waters (*cyan*) are also shown, marking the IF region of the membrane. (*d*) Distribution analysis of depth-dependent fluorescence quenching of NBD-W666C-labeled MPER peptide by spin-labeled *n*-Doxyl-PC probes. The fluorescence decays after pulsed excitation were measured for the MPER peptide in the presence of *n*-Doxyl-PC lipids (*n* equals 5, 7, 10, 12, or 14) coincorporated into POPC LUV by coextrusion. The averaged lifetimes with and without quenchers were used to generate a quenching profile (*circles*), which were fit to a sum (*solid line*) of two mirror-imaged Gaussian distributions (*dotted lines*). The transverse distributions of W666 and W666C-NBD obtained in simulation and experiment, shown respectively as shaded profiles in panels (*a*) and (*b*), correspond well to each other. To see this figure in color, go online.

several TM helices (normal lengths of TM helices range from 15 to 40 residues (58)). Increasing the length of the sliding window used in hydropathy analysis further reveals the peculiar properties of this broad hydrophobic stretch. Although increase of the window to 40 residues normally impairs the identification of known TM segments in membrane proteins, the MPER-including sequence can be identified as a favorable TM segment even with a 50-residue long window (not shown).

Previously, Hollier and Dimmock (3) used computational approaches based on structural predictions of soluble proteins to suggest that TM segments in gp41 MSD could be β-structures (Fig. S1, *right panel*). For β-structures in membranes, however, one needs to consider the thermodynamic consequences of membrane penetration of a particular conformational arrangement (see discussion in Summary section), thus the best success in sequence-based predictions is achieved using tools based on statistical analysis of known membrane proteins (59,60). Here, we use the scoring system of Freeman and Wimley (60) to examine the propensity of the MSD sequence to form TM β-strands and hairpins. Our results presented in Fig. 7 *B* indicate that the scores for strands and hairpins, obtained with 5- and 10-residue window, respectively, fall below the statistically significant thresholds for prediction of TM β-segments.

For membrane-inserting peptides or proteins one needs to explicitly consider stable IF conformations, which could be separated from the TM conformation by an energy barrier (61–63). Thus, it is not surprising that the peptide in MPER+LUV sample can be stuck in a relatively deep free energy well of the IF conformation. Our lipid titrations (Fig. S1) clearly indicate that the energy level for this IF conformation (8 kcal/mol) is comparable to those estimated using the IF Wimley-White scale (Fig. 7 *B*). The results obtained with the differential TM-IF scale is shown in Fig. 7 *D*. Note that one needs to exercise caution in direct comparison of the IF and TM free energies, as they normally have different reference points if additional folding is involved (33,62). Nevertheless, our analysis confirms the thermodynamic reasons behind the observed conformational plasticity of MPER-derived peptide in lipid bilayers.

SUMMARY

Membrane interactions of the gp41 MSD

What are the implications of the results reported in this work for the membrane topology and physiological action of gp41? Is it conceivable that the MPER sequence adopts a TM conformation at least at some point during viral fusion? What other potential TM segments can be identified with hydropathy analysis?

In the traditional topological model of the gp41 MSD, the MPER sequence has an IF location and is adjacent to a single TM helix consisting of residues 684–705, with the rest of the C-terminal sequence being completely intracytoplasmic (Fig. S1, *left panel*). To explain the external exposure of the KE (residues 721–742), Hollier and Dimmock (3) proposed an alternative model in which the membrane is spanned by three β-strands: 684–694; 695–705; and 747–757 (Fig. S1, *right panel*). Although resolving the topological conundrum by placing the KE extracellularly, this model is not supported by knowledge-based prediction algorithms for membrane proteins (Fig. 7 *C*). Moreover, it violates the basic thermodynamic principles of protein-membrane interactions. Specifically, the penetration of a nonhydrogen bonded peptide backbone into the hydrocarbon core of the lipid bilayer

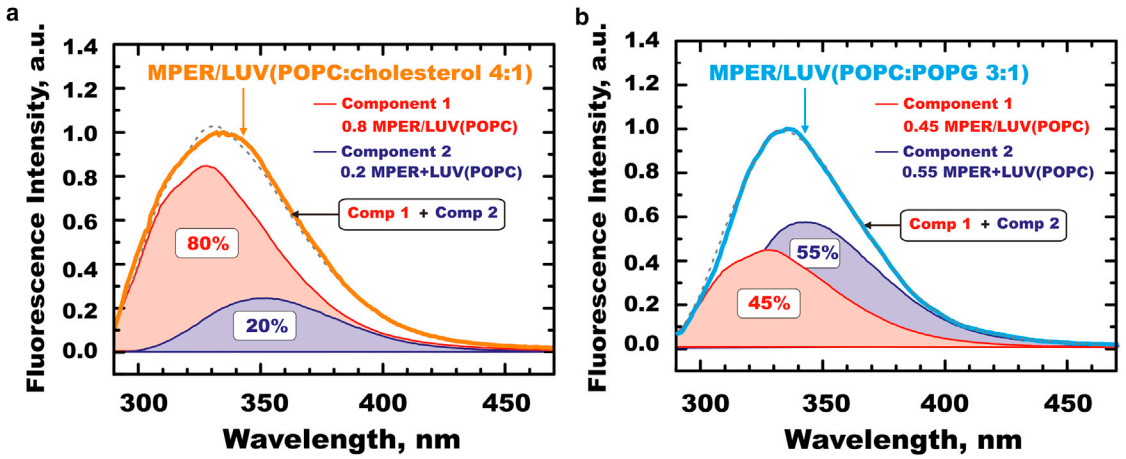

FIGURE 6 Effect of lipid composition on the spectral properties of MPER tryptophan fluorescence. The peptide was coextruded with liposomes containing POPC/cholesterol molar mixture 4:1 (*a*) POPC/POPG molar mixture 3:1 (*b*). Peptide and total lipid concentration were 2 μM and 1 mM, respectively. The observed spectra (*solid lines*) can be approximated by the combinations of individual spectra (*dashed lines*) measured in POPC (Fig. 1), which correspond to putative TM and IF conformations of MPER peptide (*shaded areas*). See text for details. To see this figure in color, go online.

carries an enormous thermodynamic penalty (45,46,54), resulting in two energetically feasible conformations of the TM sequences: α-helical bundle or a closed β-barrel (not an open-ended β-strand). Even a hydrogen-bonded helical backbone has a strong unfavorable contribution to the free energy of TM partitioning of ~2 kcal/mol per residue (57).

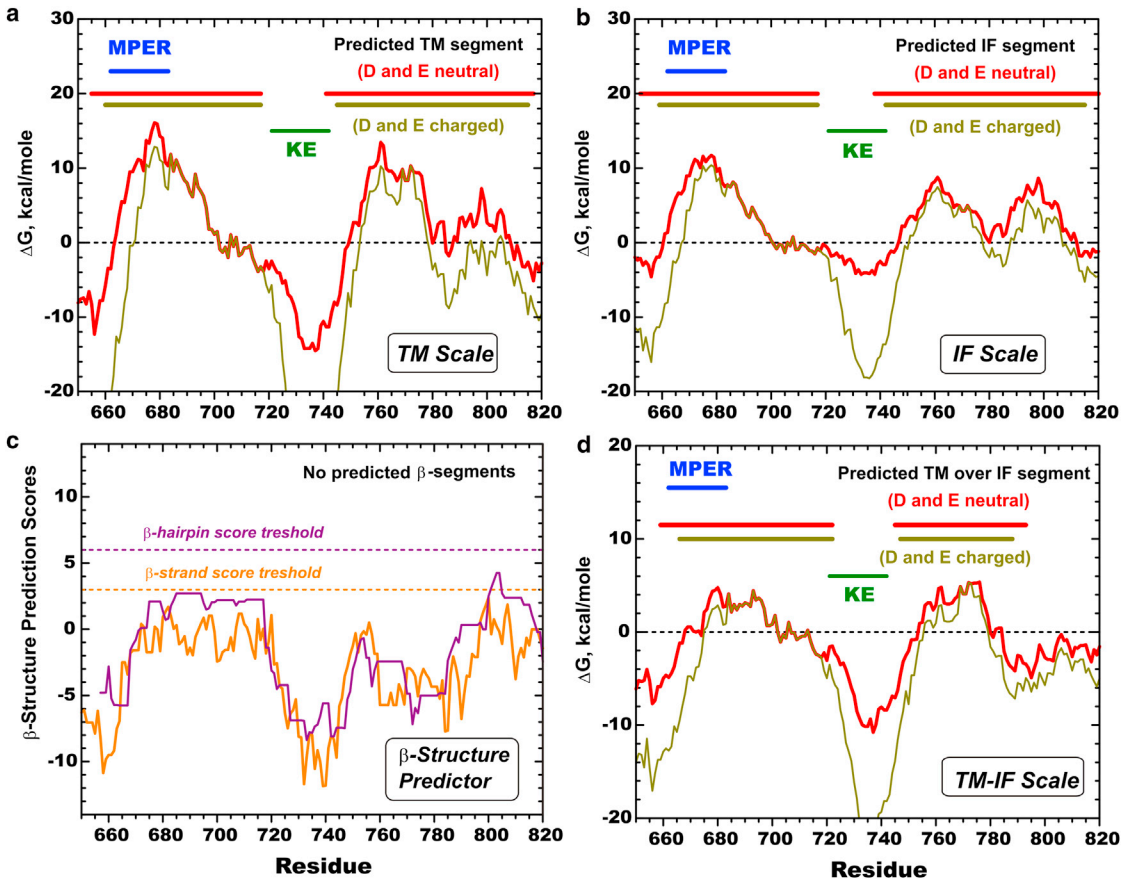

FIGURE 7 Sequence-based predictions of membrane interactions of gp41 MSD based on hydropathy analysis using the Wimley-White experimental hydrophobicity scales (9) (*a*, *b*, *d*) and β-structure predictions (*c*) performed with the MPEx web tool (http://blanco.biomol.uci.edu/mpex/ (55)). See text for details. To see this figure in color, go online.

Traditional hydropathy scales are side-chain-only scales and do not account for this contribution, whereas the Wimley-White octanol scale used in this study is a whole-residue scale (9) and produces more realistic predictions of TM segments (56).

Our hydropathy analysis of the MSD of gp41 from HIV B9.6 reveals two segments where TM helices are likely (Fig. 7, *A* and *D*): one that includes the sequence of MPER and that of the traditional TM helix and another located on the C-terminal side of the KE sequence. Note that the MPER region coincides with the maximum of the free energy profile, indicating that the TM topology of MPER is even more likely than that of the neighboring traditional TM segment. In addition, this analysis does not account for the possible formation of salt bridges, such as the one observed between E662, D664 and K665 in our MD run (Fig. S5), which will result in making this region even more favorable for TM partitioning. Thus, it is quite possible that the 660–717 stretch of residues contains not a single TM helix, but two, thus explaining the extracellular location of the KE (Fig. 8). To produce a proper intracellular location of the C-terminus, the peptide chain has to transverse the bilayer once more, which is consistent with the TM propensity of the sequence that immediately follows the KE, starting with residue 747 (*right peak* in Fig. 7 *D*).

Because the hydropathy profile for the MPER-containing segment shows a single broad peak, the turn separating the two putative TM helices is expected to be short, lacking the usual exposed loop. This is likely to put a stress on the lipid bilayer, potentially preparing it for fusion. On the other hand, it is quite possible that the entire inserted hairpin can change its topology at some prior stage or during the fusion event, producing either interfacially located helical segments (e.g., similar to those illustrated in Fig. 8, *right panel*) or some other unknown topological arrangement. One would expect that any changes in environment, such as changes in protein conformation, pH, lipid composition (e.g., Fig. 6), or proximity of other protein partners, could change the equilibrium and/or the kinetic barriers between the various topological forms of MSD of gp41. Certainly one would expect this region to play an important role as a target for antibodies, which are expected to stabilize the IF conformation of the MPER sequence, thus preventing the perturbation of the lipid bilayer required for efficient fusion.

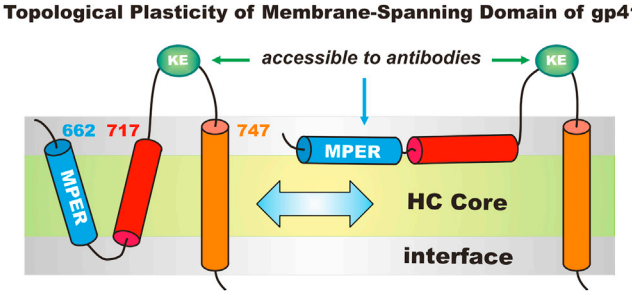

FIGURE 8 Schematic illustration of the suggested topological plasticity of the MSD of HIV-1 gp41. The TM conformation of the MPER sequence (*blue*), shown here (Figs. 2–4), leads to a new, to our knowledge, topological scheme of MD with three helical segments spanning the hydrocarbon (HC) core of the membrane (*left-hand structure*). The MPER helix and the first hydrophobic helix (*red*) form a putative TM helical hairpin, consistent with the proper exposed topology of the KE (*olive oval*). An intracellular topology of the C-terminus is assured by TM conformation of another hydrophobic helix (*orange*), predicted to start at residue 747 (Fig. 7). Because the MPER segment and the first hydrophobic helix form a continuous hydrophobic stretch (Fig. 7) and are not separated by a hydrophilic loop, the TM hairpin (residues 662–717) is not well -anchored and its topology can change to an IF (*right-hand*) configuration, e.g., as a result of interactions with antibodies or changes in lipid or protein environment. To see this figure in color, go online.

SUPPORTING MATERIAL

Five figures and one table are available at http://www.biophysj.org/biophysj/supplemental/S0006-3495(13)05849-9.

We are grateful to Drs. Likai Song and Ellis L. Reinherz for their generous gift of labeled and unlabeled MPER peptide.

This research was supported by National Institutes of Health (NIH) grant GM-069783.

REFERENCES

1. Steckbeck, J. D., A. S. Kuhlmann, and R. C. Montelaro. 2013. C-terminal tail of human immunodeficiency virus gp41: functionally rich and structurally enigmatic. *J. Gen. Virol.* 94:1–19.
2. Steckbeck, J. D., J. K. Craigo, …, R. C. Montelaro. 2011. Highly conserved structural properties of the C-terminal tail of HIV-1 gp41 protein despite substantial sequence variation among diverse clades: implications for functions in viral replication. *J. Biol. Chem.* 286:27156–27166.
3. Hollier, M. J., and N. J. Dimmock. 2005. The C-terminal tail of the gp41 transmembrane envelope glycoprotein of HIV-1 clades A, B, C, and D may exist in two conformations: an analysis of sequence, structure, and function. *Virology.* 337:284–296.
4. Steckbeck, J. D., C. Sun, …, R. C. Montelaro. 2010. Topology of the C-terminal tail of HIV-1 gp41: differential exposure of the Kennedy epitope on cell and viral membranes. *PLoS ONE.* 5:e15261.
5. Sun, Z. Y., K. J. Oh, …, E. L. Reinherz. 2008. HIV-1 broadly neutralizing antibody extracts its epitope from a kinked gp41 ectodomain region on the viral membrane. *Immunity.* 28:52–63.
6. Song, L., Z. Y. Sun, …, M. Kim. 2009. Broadly neutralizing anti-HIV-1 antibodies disrupt a hinge-related function of gp41 at the membrane interface. *Proc. Natl. Acad. Sci. USA.* 106:9057–9062.
7. Ivankin, A., B. Apellániz, …, J. L. Nieva. 2012. Mechanism of membrane perturbation by the HIV-1 gp41 membrane-proximal external region and its modulation by cholesterol. *Biochim. Biophys. Acta.* 1818:2521–2528.
8. Apellániz, B., A. Ivankin, …, J. L. Nieva. 2011. Membrane-proximal external HIV-1 gp41 motif adapted for destabilizing the highly rigid viral envelope. *Biophys. J.* 101:2426–2435.
9. Wimley, W. C., and S. H. White. 1996. Experimentally determined hydrophobicity scale for proteins at membrane interfaces. *Nat. Struct. Biol.* 3:842–848.
10. Mayer, L. D., M. J. Hope, and P. R. Cullis. 1986. Vesicles of variable sizes produced by a rapid extrusion procedure. *Biochim. Biophys. Acta.* 858:161–168.

11. Bartlett, G. R. 1959. Phosphorus assay in column chromatography. *J. Biol. Chem.* 234:466–468.
12. Ladokhin, A. S., S. Jayasinghe, and S. H. White. 2000. How to measure and analyze tryptophan fluorescence in membranes properly, and why bother? *Anal. Biochem.* 285:235–245.
13. Kyrychenko, A., Y. O. Posokhov, …, A. S. Ladokhin. 2009. Kinetic intermediate reveals staggered pH-dependent transitions along the membrane insertion pathway of the diphtheria toxin T-domain. *Biochemistry.* 48:7584–7594.
14. Kyrychenko, A., and A. S. Ladokhin. 2013. Molecular dynamics simulations of depth distribution of spin-labeled phospholipids within lipid bilayer. *J. Phys. Chem. B.* 117:5875–5885.
15. Ladokhin, A. S. 1997. Distribution analysis of depth-dependent fluorescence quenching in membranes: a practical guide. *Methods Enzymol.* 278:462–473.
16. Ladokhin, A. S. 1999. Analysis of protein and peptide penetration into membranes by depth-dependent fluorescence quenching: theoretical considerations. *Biophys. J.* 76:946–955.
17. Kyrychenko, A., D. J. Tobias, and A. S. Ladokhin. 2013. Validation of depth-dependent fluorescence quenching in membranes by molecular dynamics simulation of tryptophan octyl ester in POPC bilayer. *J. Phys. Chem. B.* 117:4770–4778.
18. Jo, S., T. Kim, …, W. Im. 2008. CHARMM-GUI: a web-based graphical user interface for CHARMM. *J. Comput. Chem.* 29:1859–1865.
19. Phillips, J. C., R. Braun, …, K. Schulten. 2005. Scalable molecular dynamics with NAMD. *J. Comput. Chem.* 26:1781–1802.
20. MacKerell, A. D., D. Bashford, …, M. Karplus. 1998. All-atom empirical potential for molecular modeling and dynamics studies of proteins. *J. Phys. Chem. B.* 102:3586–3616.
21. Best, R. B., X. Zhu, …, A. D. Mackerell, Jr. 2012. Optimization of the additive CHARMM all-atom protein force field targeting improved sampling of the backbone φ, ψ and side-chain $\chi(1)$ and $\chi(2)$ dihedral angles. *J. Chem. Theory Comput.* 8:3257–3273.
22. MacKerell, Jr., A. D., M. Feig, and C. L. Brooks, 3rd. 2004. Improved treatment of the protein backbone in empirical force fields. *J. Am. Chem. Soc.* 126:698–699.
23. Klauda, J. B., R. M. Venable, …, R. W. Pastor. 2010. Update of the CHARMM all-atom additive force field for lipids: validation on six lipid types. *J. Phys. Chem. B.* 114:7830–7843.
24. Jorgensen, W. L., J. Chandrasekhar, …, M. L. Klein. 1983. Comparison of simple potential functions for simulating liquid water. *J. Chem. Phys.* 79:926–935.
25. Grubmüller, H., H. Heller, …, K. Schulten. 1991. Generalized verlet algorithm for efficient molecular dynamics simulations with long-range interactions. *Mol. Simul.* 6:121–142.
26. Essmann, U., L. Perera, …, L. G. Pedersen. 1995. A smooth particle mesh Ewald method. *J. Chem. Phys.* 103:8577–8593.
27. Ryckaert, J.-P., G. Ciccotti, and H. J. C. Berendsen. 1977. Numerical integration of the Cartesian equations of motion of a system with constraints: molecular dynamics of *n*-alkanes. *J. Comput. Phys.* 23: 327–341.
28. Miyamoto, S., and P. A. Kollman. 1992. Settle: an analytical version of the SHAKE and RATTLE algorithm for rigid water models. *J. Comput. Chem.* 13:952–962.
29. Feller, S. E., Y. Zhang, …, B. R. Brooks. 1995. Constant pressure molecular dynamics simulation: the Langevin piston method. *J. Chem. Phys.* 103:4613–4621.
30. Martyna, G. J., D. J. Tobias, and M. L. Klein. 1994. Constant pressure molecular dynamics algorithms. *J. Chem. Phys.* 101:4177–4189.
31. Pronk, S., S. Páll, …, E. Lindahl. 2013. GROMACS 4.5: a high-throughput and highly parallel open source molecular simulation toolkit. *Bioinformatics.* 29:845–854.
32. Humphrey, W., A. Dalke, and K. Schulten. 1996. VMD: visual molecular dynamics. *J. Mol. Graph.* 14:33–38.
33. Ladokhin, A. S., and S. H. White. 1999. Folding of amphipathic α-helices on membranes: energetics of helix formation by melittin. *J. Mol. Biol.* 285:1363–1369.
34. Fernández-Vidal, M., S. H. White, and A. S. Ladokhin. 2011. Membrane partitioning: "classical" and "nonclassical" hydrophobic effects. *J. Membr. Biol.* 239:5–14.
35. Burstein, E. A., N. S. Vedenkina, and M. N. Ivkova. 1973. Fluorescence and the location of tryptophan residues in protein molecules. *Photochem. Photobiol.* 18:263–279.
36. Burstein, E. A., S. M. Abornev, and Y. K. Reshetnyak. 2001. Decomposition of protein tryptophan fluorescence spectra into log-normal components. I. Decomposition algorithms. *Biophys. J.* 81:1699–1709.
37. Burstein, E. A. 1976. Luminescence of Protein Chromophores (Model Studies). VINITI, Moscow.
38. Burstein, E. A. 1977. Intrinsic Protein Luminescence (Origins and Applications). VINITI, Moscow.
39. Reshetnyak, Y. K., and E. A. Burstein. 2001. Decomposition of protein tryptophan fluorescence spectra into log-normal components. II. The statistical proof of discreteness of tryptophan classes in proteins. *Biophys. J.* 81:1710–1734.
40. Reshetnyak, Y. K., Y. Koshevnik, and E. A. Burstein. 2001. Decomposition of protein tryptophan fluorescence spectra into log-normal components. III. Correlation between fluorescence and microenvironment parameters of individual tryptophan residues. *Biophys. J.* 81:1735–1758.
41. Ladokhin, A. S., M. E. Selsted, and S. H. White. 1999. CD spectra of indolicidin antimicrobial peptides suggest turns, not polyproline helix. *Biochemistry.* 38:12313–12319.
42. Wu, Y., H. W. Huang, and G. A. Olah. 1990. Method of oriented circular dichroism. *Biophys. J.* 57:797–806.
43. Krauson, A. J., J. He, and W. C. Wimley. 2012. Gain-of-function analogues of the pore-forming peptide melittin selected by orthogonal high-throughput screening. *J. Am. Chem. Soc.* 134:12732–12741.
44. Ladokhin, A. S., and S. H. White. 2001. 'Detergent-like' permeabilization of anionic lipid vesicles by melittin. *Biochim. Biophys. Acta.* 1514:253–260.
45. Popot, J.-L., and D. M. Engelman. 1990. Membrane protein folding and oligomerization: the two-stage model. *Biochemistry.* 29:4031–4037.
46. White, S. H., and W. C. Wimley. 1999. Membrane protein folding and stability: physical principles. *Annu. Rev. Biophys. Biomol. Struct.* 28:319–365.
47. White, S. H., A. S. Ladokhin, …, K. Hristova. 2001. How membranes shape protein structure. *J. Biol. Chem.* 276:32395–32398.
48. Klug, C. S., and J. B. Feix. 2008. Methods and applications of site-directed spin labeling EPR spectroscopy. *Methods Cell Biol.* 84:617–658.
49. London, E., and A. S. Ladokhin. 2002. Measuring the depth of amino acid residues in membrane-inserted peptides by fluorescence quenching. *Curr. Top. Membr.* 52:89–115.
50. Posokhov, Y. O., and A. S. Ladokhin. 2006. Lifetime fluorescence method for determining membrane topology of proteins. *Anal. Biochem.* 348:87–93.
51. Kyrychenko, A., and A. S. Ladokhin. 2014. Refining membrane penetration by a combination of steady-state and time-resolved depth-dependent fluorescence quenching. *Anal. Biochem.* 446:19–21.
52. Ladokhin, A. S. 1999. Evaluation of lipid exposure of tryptophan residues in membrane peptides and proteins. *Anal. Biochem.* 276:65–71.
53. Reference deleted in proof.
54. White, S. H., W. C. Wimley, …, K. Hristova. 1998. Protein folding in membranes: determining energetics of peptide-bilayer interactions. *Methods Enzymol.* 295:62–87.
55. Snider, C., S. Jayasinghe, …, S. H. White. 2009. MPEx: a tool for exploring membrane proteins. *Protein Sci.* 18:2624–2628.

56. Jayasinghe, S., K. Hristova, and S. H. White. 2001. Energetics, stability, and prediction of transmembrane helices. *J. Mol. Biol.* 312:927–934.

57. Kyrychenko, A., M. V. Rodnin, …, A. S. Ladokhin. 2012. Thermodynamic measurements of bilayer insertion of a single transmembrane helix chaperoned by fluorinated surfactants. *J. Mol. Biol.* 416: 328–334.

58. Jayasinghe, S., K. Hristova, and S. H. White. 2001. MPtopo: a database of membrane protein topology. *Protein Sci.* 10:455–458.

59. Wimley, W. C. 2002. Toward genomic identification of β-barrel membrane proteins: composition and architecture of known structures. *Protein Sci.* 11:301–312.

60. Freeman, Jr., T. C., and W. C. Wimley. 2010. A highly accurate statistical approach for the prediction of transmembrane beta-barrels. *Bioinformatics.* 26:1965–1974.

61. Ladokhin, A. S., R. Legmann, …, S. H. White. 2004. Reversible refolding of the diphtheria toxin T-domain on lipid membranes. *Biochemistry.* 43:7451–7458.

62. Ladokhin, A. S., and S. H. White. 2004. Interfacial folding and membrane insertion of a designed helical peptide. *Biochemistry.* 43:5782–5791.

63. Posokhov, Y. O., M. V. Rodnin, …, A. S. Ladokhin. 2008. Membrane insertion pathway of annexin B12: thermodynamic and kinetic characterization by fluorescence correlation spectroscopy and fluorescence quenching. *Biochemistry.* 47:5078–5087.